Available online at www.sciencedirect.com

SciVerse ScienceDirect

Procedia IUTAM 3 (2012) 91 – 99

Procedia IUTAM

www.elsevier.com/locate/procedia

IUTAM Symposium on Linking Scales in Computations: from Microstructure to Macro-Scale Properties

Mechanical Behavior of Non-bonded Fiber Networks in Compression

R.C. Picu*

Department of Mechanical, Aerospace and Nuclear Engineering, Rensselaer Polytechnic Institute, Troy, NY 12180

Abstract

The mechanical behavior of an ensemble of fibers which are not bonded to each other subjected to compression is studied using a numerical model. It is shown that the stress-strain curve is a power law and the strain energy is stored predominantly in the bending deformation mode of the fibers. Hysteresis is observed when the system is subjected to cyclic loading-unloading, with a stable hysteresis loop being obtained after few cycles. The deformation is not smooth; rather it is dominated by instabilities which lead to pronounced stress drops. These instabilities are due to relative fiber sliding and rearrangement and a correlation is observed between stress drops and collective sliding events. The resulting jerky flow is observed even in absence of friction between fibers and is a result of the evolution of the system over a rough energy landscape during compression.

Keywords: fiber networks; entangled materials; avalanches.

**Corresponding author*. Tel: 1(518) 276-2195; Fax: 1(518) 276-6025
E-mail address: picuc@rpi.edu

 doi:10.1016/j.piutam.2012.03.007

1. Introduction

Fibrous materials are frequently encountered in the engineering and biological worlds. Engineering materials made from fibers are rubber, cellulose and paper, cloth, most types of insulation and various consumer products such as wipes and baby diapers. Cellulose fibers are used in many applications, including paper, construction materials and various types of insulation products. In these examples fibers are randomly distributed and randomly oriented. These may be bonded to each other, as in the case of paper, or non-bonded (this configuration is occasionally denoted in the literature as "entangled") as in the case of insulation felt. Cloth is usually woven and hence the fiber distribution is not random. Rubber is composed from macromolecules linked to each other at cross-linking points. The cross-link density can be controlled and densely cross-linked rubbers as well as sparsely cross-linked rubbers are produced, with dramatically different mechanical properties.

Fiber networks are frequently encountered in the biological world as well. Most connective tissues in the human and animal bodies are made from fibers such as collagen and elastin. Examples are tendons, cartilage, some components of the skin and the eye cornea. In some cases, fibers are randomly distributed while in others, a regular arrangement is observed. Likewise, both cross-linked and non-cross-linked situations are encountered. Note that in this description the notion of cross-linking, which is commonly used when referring to molecular networks, is employed in a broader sense, being applied to macroscopic fibers as well.

Molecular scale fibers, i.e. filaments which are made from single molecules or from bundles of few molecules, are subjected to thermal fluctuations. Hence, their free energy includes an entropic component. Additional components of the free energy are enthalpic and are due to stretching and bending of the filament. In single-molecule filaments such as in rubber, the enthalpic contribution is usually neglected in models. Larger fibers, including collagen and elastin filaments, are predominantly enthalpic. These can be divided in flexible and semi-flexible, function of the relative contribution of the bending mode to the overall stored energy. Specifically, bending is neglected in flexible fibers, but is important in many fibers of industrial use, such as cellulose and polymeric fibers used in consumer products.

The mechanics of bonded networks was studied extensively and several reviews have been published [e.g. 1,2]. The bonds are permanent and may transmit both moments and forces, or just forces. Some special types of bonds may have a complex internal constitutive behavior; an important example is that of the cytoskeleton which is a network of F-actin fibers. The F-actin filaments are bonded by connecting proteins which unravel when forces are applied [3] leading to a complex mechanical signature.

The mechanical behavior of bonded networks is essentially elastic, the strain recovering fully upon unloading due to the fact that the bonds prohibit fiber rearrangement, i.e. microstructural evolution. Interestingly, the network stiffness depends on two parameters: the fiber density and the relative importance of bending relative to the stretching mode. Dense networks made from fibers stiff in bending (which deform mostly axially) have stiffness which scales linearly with the density. In the opposite case, the stiffness scales as ρ^8, where ρ is the network density. This very strong sensitivity to density is surprising and allows living systems to acquire/reduce stiffness with a minimal addition/reduction of mass.

The mechanics of non-bonded networks has been less studied and, as discussed in this article, is significantly more complex than that of bonded networks. The primary reason is that in non-bonded networks the microstructure changes during deformation due to fiber rearrangement. The contacts between fibers are temporary and transmit only forces. If friction is present, as in most real systems, small axial forces can be transmitted too. The published experimental [4,5], numerical [6,7] and analytical [8,9] works investigating the mechanical behavior of these systems have focused on uniaxial, biaxial or triaxial compression, which is motivated by industrial processes. The experimental works indicate that the stress-

strain relation is a power function with an exponent ranging from 2 to 6, depending on the type of test, initial sample density, etc. Hysteresis is commonly observed when performing cyclic loading. Time-dependent response, creep and relaxation, is common and is generally assigned to the time-dependent mechanical behavior of fiber-fiber contacts. The system should not exhibit rate sensitivity if fibers are elastic and no dissipation takes place at contacts. A small number of models exist and most make simplifying assumptions about the network evolution. For example, no available model takes into account the fiber rearrangement associated with the relative sliding of fibers. These models [8,9] predict that the exponent of the stress-strain power law is equal to 3. This is not in very good agreement with experimental observations as in most cases the exponent results significantly larger than 3 [4,5].

Several numerical results concerning the behavior of non-bonded fiber systems are reviewed in this article. The detailed discussion is presented in [10,11]. These models reproduce the power law dependence of stress on strain with the exponent being in the experimental range. Hysteresis is also reproduced. It is observed that sliding at fiber contacts and fiber rearrangement is important and leads to structural instabilities which are observed at the system scale as stress drops. The power law stress-strain dependence is the envelope of the stress-strain curve exhibiting instabilities.

2. Model

Semiflexible fibers are modeled with the bead-spring model frequently used in polymer physics [e.g. 12]. Each fiber is represented by a chain of beads connected by harmonic springs. The energy associated 2 respectively, where r and r_0 are the current and reference distance between successive beads, and θ and θ_0 are the current and reference angles made by successive bonds along the fiber. A shifted Lennard-0. The potential is truncated at its minimum to eliminate the cohesive effect, and $\theta_0 = \pi$, i.e. fibers are straight when unloaded. s and e become the units of length and energy of the problem, respectively. The 0. The elastic contact between two cylinders of same radius is described by Hertz's formula. Requiring that the contact energy computed with this continuum model equals the energy of non-bonded interactions evaluated with the LJ potential at same relative bead displacement (inter-penetration of fibers), leads to a relationship between the reduced Young's modulus of the fiber, $E/(1 - \nu^2)$ (ν is Poisson's ratio), and the energy constant, e: $E/(1 - \nu^2) \sim 420.4e/s^3$. Further, approximating $1 - \nu^2 = 1$, one $EA = 0.28s$. These considerations allow mapping the discrete model of a fiber to a continuous cylindrical Euler-Bernoulli beam of radius r_0. Furthermore, the axial stiffness is large enough for fibers not to cross each other. It was tested (by increasing the bead number density along each fiber) that the roughness due to the discrete representation used for fibers does not lead to artificial friction or adhesion of fibers in contact.

Initial configurations are obtained by growing straight fibers with random orientations in a large $2/2$ is the area of the fiber section, L_0 is the fiber length and L is the size of the simulation box. In these simulations, $N = 1200$, $L_0 = 50s$ and the size of the model when fibers are generated is $L = 509.7$s. The resulting configuration is subjected to stepwise hydrostatic compression. In order to avoid artifacts introduced by the periodic boundary conditions, the size of the simulation box at the maximum density (maximum compression) is kept larger than L_0.

The system is loaded by imposing displacements along the model boundaries; the fibers move as in molecular dynamics. The equations of motion include a small damping term which cools-down the system towards the zero Kelvin equilibrium state. Coulomb friction between fibers may be included, however, the results reported here correspond to a vanishing friction coefficient, $\mu = 0$. The deformation is imposed in small steps and the system is allowed to reach its static equilibrium state after each step. The sequence of these equilibrium configurations is considered the quasi-static, athermal trajectory of the system.

The deformation is described by a spherical deformation gradient tensor $\mathbf{F} = q\mathbf{I}$, where $\mathbf{I}$ is the identity matrix and q is a variable parameter. The resulting dilatation strain, Δ, which is the trace of the Green strain, $\mathbf{E}$, is $\Delta = (3/2)(q^2-1)$. Parameter q is related to the density as $q=(\rho_0/\rho)^{1/3}$, with ρ and ρ_0 being the current and reference densities ($\rho_0 = 1$). The Cauchy stress is evaluated as

$$\boldsymbol{T} = \frac{1}{\det \mathbf{F}} \mathbf{F} \cdot \frac{\partial U}{\partial \mathbf{E}} \cdot \mathbf{F}^T, \tag{1}$$

with $\langle in \rangle$ being the strain energy density which is computed by summing up contributions of bending, axial, and contact energies over all interactions. $\mathbf{T}$ results a spherical tensor with diagonal components given by

$$\sigma = -3\rho^2 \frac{\partial U}{\partial \rho}. \tag{2}$$

During deformation, contacts are created between fibers. The plane of a contact is the common tangent plane of the two beads forming the contact. The sliding distance in given load increment in each contact, S, is defined as the norm of the component of the vector of relative displacement projected in the plane of the contact. The mean sliding distance is computed as the average over the entire population of contacts in the current state, $\langle S \rangle$.

3. Results

Figure 1 shows the variation of the stress (pressure) as the system is subjected to triaxial compression, function of the dilatation strain, Δ. Three curves are shown: that labeled "Transient," corresponds to the first loading-unloading cycle, while the two curves labeled "Stable" have been obtained in simulations performed with different initial systems (different realizations) and after the loading-unloading hysteresis loop has stabilized. The two "Stable" curves essentially overlap, while some degree of softening is associated with cycling.

As the system is compacted from the sparse state in which fibers are generated, the percolation limit and then the stiffness percolation limit are reached. At stiffness percolation, the stress increases abruptly, as shown by the vertical lines in Fig. 1. The subsequent behavior is well described by the power law $\sigma \sim \langle \Delta \rangle^{5.46}$. For the range of densities considered, this is equivalent to $\sigma \sim \langle \rho \rangle^{4.1}$. This exponent is larger than that predicted theoretically using a mean field model by van Wyk [8]. As mentioned in the Introduction, the exponents measured in experiments range from 2 to 6 [5], function of the initial mass of the sample and the type of material used for fibers. In fact, the model proposed by Toll [9] predicts an exponent of 5 for quasi-two-dimensional system, i.e. when the network is almost flattened out.

In [11] it was shown that the exponent of the stress-strain function depends significantly on the bending stiffness of the fibers. Specifically, increasing/decreasing k_b leads to an increase/decrease of the exponent. This effect is shown in Fig. 2 where the bending stiffness coefficient is increased and decreased by an order of magnitude, in separate simulations. The large value of k_b corresponds to the stress-strain relation $\sigma \sim \langle \Delta \rangle^{7.5}$, while the low value corresponds to $\sigma \sim \langle \Delta \rangle^{4.2}$. The corresponding dependence of

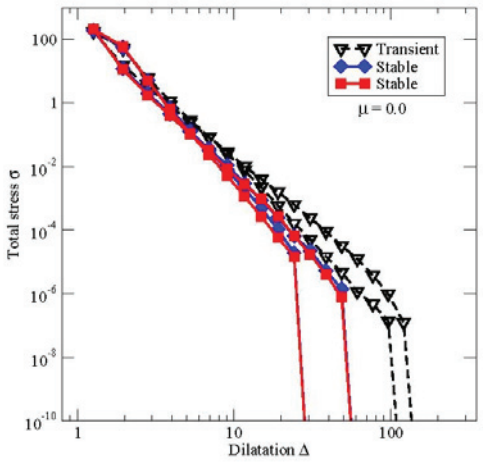

Fig. 1. Stress (pressure) – strain (dilatation) curves for the triaxial loading-unloading of a system of athermal fibers. The black curve is the first loading-unloading cycle. The other curves are "Stable" hysteresis loops obtained with different realizations of the system.

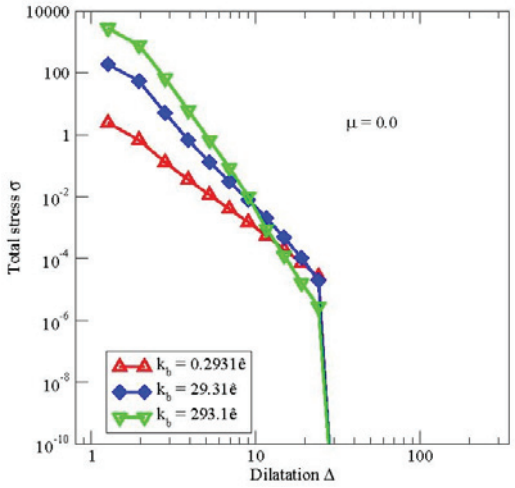

Fig. 2. Stress (pressure) – strain (dilatation) curves for the triaxial compression of systems of fibers with different bending stiffness. The stress-strain curves are power functions, but the exponent depends on the fiber bending stiffness.

The behavior shown in Fig. 2 can be explained, in part, by analyzing the partition of energy in bending and axial deformation modes of fibers. Reducing the bending stiffness enables more strain energy to be stored in the bending mode, while increasing l_b has the opposite effect. The system behaves as if the two deformation modes (bending and axial) are coupled in series.

The effect of friction on the overall behavior was also studied in [10,13]. It was observed that accounting for friction does not change the results discussed here; the stress-strain curve remains a power function and the exponent does not change significantly. Of course, the stress values change when friction is taken into consideration.

The major difference between bonded and non-bonded networks is the fact that in non-bonded networks fibers are free to slide relative to each other. As the system is compacted, new contacts form and the stiffness increases. Clearly, this takes place in bonded networks too; fibers interact initially only at the bond sites but new, non-bonded, contacts form when large deformations are imposed. This is usually neglected in models of bonded networks, both analytic and numeric. One may also speculate that this effect is secondary in dense bonded networks, leading to a marginal increase of the stiffness from the already relatively high value due to the presence of the bonds, but the effect of fiber excluded volume in bonded networks was not studied systematically.

As discussed in the Introduction, the modulus of a bonded network scales linearly with the density at large l_b and ρ, and scales as ρ^8 at small l_b and ρ. The non-bonded network considered here is compacted, so ρ varies in a relatively large range, while l_b is constant. If the behavior of bonded and non-bonded networks is similar, one expects that the modulus should change gradually from a power function with a large exponent to a linear variation with ρ as the system is compacted. In fact, the bulk modulus of the system can be described at all ρ by the function $\rho^{4.75}$. This holds for approximately two orders of magnitude of variation of Δ. To check that the expected behavior is reproduced if the network is bonded, rigid bonds were introduced between all fibers in contact at a specified value of the density, therefore transforming the non-bonded network into a bonded one. The stiffness is probed by applying a small compression increment to the resulting system. Figure 3 shows the effect of this transformation; the slope of the stress-strain curves increases after the artificial bonding to a large value close to 8. This behavior is observed repeatedly if bonding is performed at different compaction stages (Fig. 3).

It is interesting to compute the amount of relative sliding taking place in each load increment. To this end, the measure S described in Section 2 is evaluated from the numerical model and its distribution function and mean, $\bar{S}$, are computed. S is computed relative to a configuration taken as reference. This quantity is Poisson distributed [11], so the mean is sufficient to characterize the evolution of the distribution function with strain. Figure 4 shows the variation of $\bar{S}$ with the dilatation strain (blue dashed line), where the sliding distance is evaluated in each step relative to the configuration in the previous loading step. It is seen that as the system is compacted, the mean sliding distance per load increment is essentially constant. However, beyond a certain compaction stage, large spikes are observed in $\bar{S}$. This indicates that "avalanches," i.e. intermittent fiber sliding and rearrangement take place in certain load increments. Between the load steps in which avalanches are seen, the value of $\bar{S}$ is essentially identical to that obtained at larger Δ when no avalanches take place. It is interesting to note that the fiber orientation remains random during an avalanche. To our knowledge, this is the first observation of intermittent dynamics in this type of systems. Intermittent dynamics is frequently observed in random discrete systems such as granular materials and dislocation structures, and in earthquake dynamics and damage accumulation in brittle materials.

The stress-strain curve for this system is also shown in Fig. 4 (red continous line). The stress increases continously as the system is compacted (Δ decreases), but in the steps in which $\bar{S}$ has large spikes, the stress drops. This is a manifestation of the instability associated with the fiber rearrangmenet occruing during an avalanche. The black dashed curve overlapping the stress-strain curve is identical to the loading branch of the curve labeled "Stable" in Fig. 1. The curves in Fig. 1 are smooth since that data is sampled less frequently and an averaging is performed over few neighboring data points (window averaging).

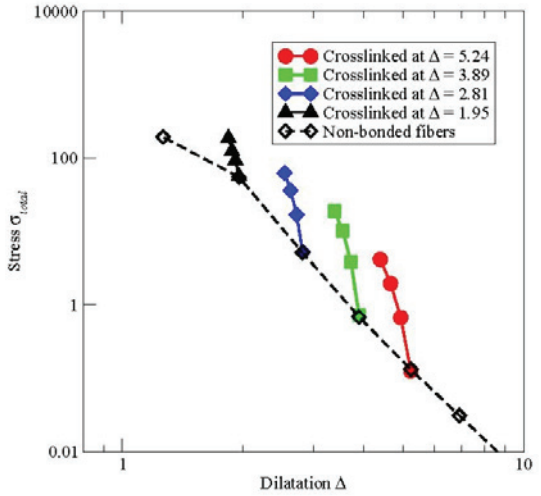

Fig. 3. Stress-strain curves resulting after introducing artificial permanent bonds in the non-bonded network at various stages of compression. The open symbols represent the curve obtained if no permananet bonds are introduced (Fig. 1).

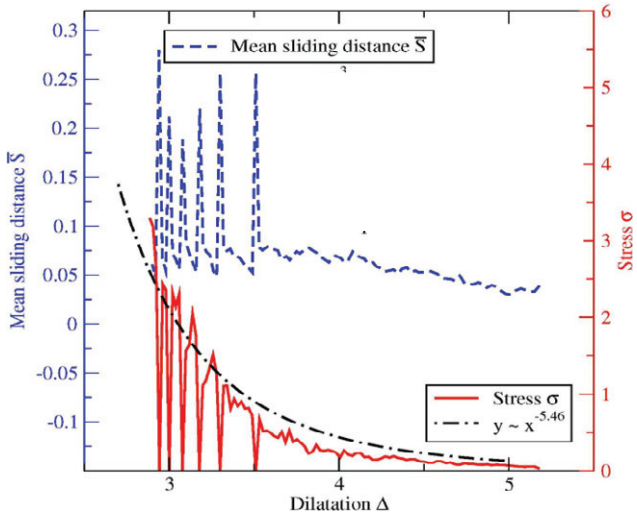

Fig. 4. Variation of the hydrostatic stress (continuous red line, and right vertical axis), and of the mean sliding measure (dashed blue line, and left vertical axis) with the dilatation strain Δ, or density ρ, top axis. The units for σ and S are e/s^3 and s, respectively. The dash-dot black line shows the loading branch of the "Stable" stress-strain curve in Fig. 1.

The variation of the total strain energy density U with Δ is shown in Fig. 5. The function is smooth for Δ>3.5 and exhibits serrations for smaller Δ. The presence of these drops (which coincide with the spikes observed in S) shows that this slowly driven system evolves over a rough energy landscape. The energy is purely elastic and its dependence on strain is not monotonic even at small deformations since the relative positions of fibers may change.

A large number of fibers are involved in an avalanche. The inset to Fig. 5 shows the fraction of all fibers in the system containing at least a contact which slides more than $S = S'$, $n(S>S')/N$, versus S'. The two curves correspond to the load step at Δ=3.53, when an avalanche is seen, and to the immediately following load step in which there is no avalanche. While in the load step without avalanche no fiber slides more than $S = 0.4s$, during an avalanche 90% of the fibers slide more than this threshold and 1/3 of fibers slide even more than $0.8s$.

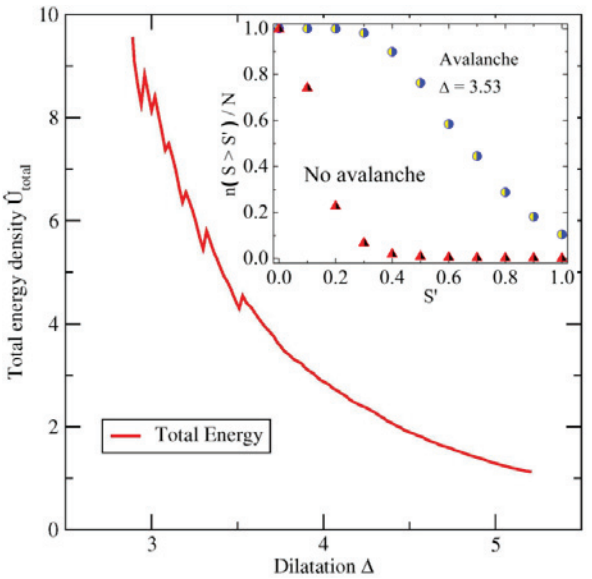

Fig. 5. Variation of the total strain energy density U with the strain Δ. Serrations are observed in the energy curve. The inset shows the fraction of chains having at least a contact which slides more than S', $n(S>S')/N$, versus S', for two load steps, with and without avalanches.

4. Conclusions

Non-bonded (entangled) and bonded fiber networks respond to mechanical loading differently. When subjected to compression, the stress varies as a power function of the fiber density in both systems, but the exponents are different even when the geometry and loading conditions are similar. In the case of the non-bonded networks, the exponent depends on the fiber bending stiffness, increasing as the bending stiffness increases. Changing the ratio of the bending and axial stiffness of fibers also changes the energy partition in the bending and axial deformation modes of the fibers; the system behaves as if the two modes were connected in series.

A phenomenon specific to non-bonded networks is the evolution of the microstructure due to relative fiber sliding. This process leads to internal instabilities which cause stress oscillations. Once the density becomes large enough during compaction, the stress-strain curve becomes serrated and the mean sliding

distance per loading step exhibits large spikes. Analyzing the statistics of the sliding events sheds light on the nature of these instabilities. The magnitude of these events is spatially correlated up to a distance equal to the fiber length, L_0. These correlations indicate that entire fibers move (as opposed to a localized fiber deformation). The loss of correlation beyond L_0 indicates that the motion of neighboring fibers is not correlated. It is also important to note that a large number of fibers in the ensemble contribute to sliding, so the phenomenon is not localized in a band or "transformation zone." These conclusions cannot be verified against experimental observation since no such data exist at this time.

The deformation of fiber networks, both bonded and non-bonded, is complex due the discrete nature of these systems and to the non-local interaction of fibers. As with many systems of this type, using mean field considerations to derive effective constitutive laws for the ensemble of fibers does not lead to reliable results and the link between the system-scale mechanical behavior and the microstructure remains elusive. Numerical models of the type described here and in the cited references provide useful information on the statistics of the deformation, which will assist in the derivation of microstructure-informed constitutive descriptions for these materials.

References

[1] Rigdahl M, Hollmark H, Network mechanics. In Bristow JA, Koleth P, editors. *Paper structure and properties*, Marcel Dekker; 1986, p. 241-66.

[2] Picu RC. Mechanics of random fiber networks – a review. *Soft Matter* 2011; **7**:6768-85.

[3] Broedersz CP, Storm C, MacKintosh FC. Nonlinear elasticity of composite networks of stiff biopolymers with flexible linkers. *Phys. Rev. Lett*. 2008; **101**: 118103(1-4).

[4] Masse J, Salvo L, Rodney D, Brechet Y, Bouaziz, O. Influence of relative density on the architecture and mechanical behaviour of a steel metallic wool. *Scripta Mat*. 2006; **54**: 1379-83.

[5] Poquillon D, Viguier B, Andrieu E. Experimental data about mechanical behavior during compression tests for various matted fibres. *J. Mat. Sci*. 2005; **40**:5963-70.

[6] Rodney D, Fivel M, Dendievel R. Discrete modeling of the mechanics of entangled materials. *Phys. Rev. Lett*. 2005; **95**:108004(1-4).

[7] Durville D. Numerical simulations of entangled material mechanical properties. *J. Mat. Sci*. 2005; **40**: 5941-48.

[8] vanWyk CM. Note on the compressibility of wool.. *J. Textile Inst*. 1946; **37**: T285-92.

[9] Toll S. Packing mechanics of fiber reinforcements. *Polymer Eng. Sci*. 1998; **38**: 1337-45.

[10] Subramanian G, Picu RC. Mechanics of three-dimensional, non-bonded random fiber networks. *Phys. Rev. E* 2011; **83**: 056120(1-9).

[11] Picu RC, Subramanian G. Correlated heterogeneous deformation of entnagled fiber networks. *Phys. Rev. E* 2011; **84**: 031904(1-4).

[12] Picu RC, Loriot G, Weiner JH. Towards a unified view of stress in small molecular and macromolecular liquids. *J. Chem. Phys*. 1999; **110**: 4678-86.

[13] Barbier C, Dendievel R, Rodney D. Role of friction in the mechanics of non-bonded fibrous materials. *Phys. Rev. E* 2009; **80**: 016115(1-6).